PCCP

Quantum mechanical study of photodissociation of oriented ClNO(S_1)

Hua Guo[a] and Tamar Seideman[b]

[a] *Department of Chemistry, University of New Mexico, Albuquerque, New Mexico 87131, USA*
[b] *Steacie Institute, National Research Council, Ottawa, Ontario, K1A 0R6, Canada*

Received 1st September 1998, Accepted 5th November 1998

We report a full-dimensional, quantum mechanical study of the photodissociation dynamics of ClNO(S_1) with the complete (JMK) selection of the parent state. Total cross-sections, product-state distributions, and photofragment angular distributions are computed. The influence of the parent rotation and orientation on the dissociation dynamics is analysed. The calculations were carried out using a time-independent propagation method based on Chebyshev polynomials, which combines the accuracy and efficiency essential for the type of problem considered.

1 Introduction

A major advance in studying reaction dynamics has been the ability to orient or align isolated molecules in the gas phase. The selection of molecular orientation or alignment has important implications in chemical reactions because many are stereo-selective, that is, favoured at certain angles of approach. Therefore, by selecting the orientation or alignment of the reactants, one can potentially enhance the reactivity or even control the branching of final products. The orientation or alignment of molecules can be achieved in a number of ways. The two most widely employed schemes are magnetic-state selection, either in an electric hexapole field[1–3] or optically,[4] and alignment in a strong DC field,[5,6] termed "brute force" alignment. Other schemes include collisional alignment,[7,8] cluster- or surface-assisted orientation[9–11] and the recently introduced schemes for aligning molecules in an intense laser field.[12,13]

Ample examples have been reported on the stereo-control of gas-phase and gas-surface reactions.[2,3] Less attention has, however, been devoted to the possibility of extracting useful information regarding excited states through photodissociation of (JMK)-selected parent molecules,[14,15] this opportunity being unique to fully state-selected experimental schemes.[16–18] Ref. 19, for example, showed that fragment angular distributions following photodissociation of single (magnetic- as well as energy-level-selected) quantum states provide information regarding the transition dipole function coupling the bound and dissociative states. The possibility of determining the dynamical photodissociation transition matrix elements by combining measurements and calculations of (JMK)-selected angular distributions was illustrated in ref. 20.

Our ability to extract information from measured data relies on the availability of accurate and efficient numerical methods for calculation of both integrated and differential cross-sections. Although the quantum mechanical theory of photodissociation was formulated earlier on,[14,15] full-dimensional calculations for realistic systems proved difficult. This is particularly true since, for calculation of vector properties of photofragmentation processes and for elucidation of the dynamical information contained in fully state-selected cross-sections, it is essential to take the total angular momentum into proper account. In the past few years, much effort has been devoted to the study of vector properties of dissociation processes and their relationship to the dissociation dynamics.[21–26] Recent experimental advances in selecting isolated molecules provide additional incentives to investigate the dissociation of molecules in selected initial rotational quantum states.[19] These advances call for the development of efficient numerical schemes for calculation of the photodissociation dynamics. In this work, we introduce an efficient propagation approach based on Chebyshev polynomials[27] and apply it to the photodissociation dynamics of rotating ClNO.

The ClNO system has been investigated experimentally in great detail.[28,29] The absorption spectrum for the first singlet-excited state consists of defused and overlapping vibrational bands.[30] The rotational distribution of the NO fragment is highly inverted,[31–34] underscoring the large torque experienced by the fragment in the exit channel.[35] The coupling between the rotational and vibrational degrees of freedom of the NO fragment was found to be relatively weak and the vibrational dynamics is nearly adiabatic. Quantum mechanical studies of the ClNO dissociation have been reported by several groups. Schinke and co-workers have carried out both two-[36] and three-dimensional[37] calculations using an *ab initio* potential-energy surface. The quantum mechanical results agree well with experimentally measured total and partial cross-sections. Manthe *et al.*[38] reported a time-dependent multi-configuration Hartree study using a different fit to the same set of *ab initio* data. Model studies were reported also for the photodissociation on the lower T_1 state, which is dominated by slow predissociation.[39,40] So far, theoretical studies of the ClNO photodissociation have been restricted to zero total angular momentum and concentrated on angle-averaged observables.

Very recently, the photodissociation of single (JMK) quantum states of ClNO was studied experimentally by Baugh *et al.*[41] and found to exhibit rich dynamics which was not resolved in less detailed measurements. These authors were able to measure the angle-resolved product-state distributions from the dissociation of rotational state-selected parent molecules using hexapole focusing.[17] The present study complements the work of Baugh *et al.*[41] by studying quantum mechanically the ClNO($S_0 \rightarrow S_1$) total and partial cross-sections and the photofragment angular distributions for a number of (JMK)-initial states. These results are expected to

reveal the effects of the initial rotation and orientation of the parent molecule on the dissociation dynamics. This work is organized as follows. The general theory of photodissociation is briefly reviewed in the next section. In Section III, we outline the implementation of the theory in the discrete variable representation and in the Chebyshev order domain. The calculated results are presented in Section IV, and the conclusions are given in Section V.

II Theory

A Hamiltonian

The coordinate system describing the triatomic molecule is that of Jacobi, in which the N—O distance is denoted by r, the distance between Cl and NO centre-of-mass by R, and the angle between the $\boldsymbol{r}$ and $\boldsymbol{R}$ vectors by χ. The body-fixed (BF, unprimed) frame places the z axis along the $\boldsymbol{R}$ vector and the y axis along the space-fixed (SF, primed) $x'y'$ plane.[42] The molecular Hamiltonian corresponding to the volume element of $\sin\chi\,\mathrm{d}\chi\,\mathrm{d}r\,\mathrm{d}R$ is given as

$$\hat{H} = -\frac{\hbar^2}{2\mu_R}\frac{\partial^2}{\partial R^2} - \frac{\hbar^2}{2\mu_r}\frac{\partial^2}{\partial r^2} + \left(\frac{1}{2\mu_r r^2} + \frac{1}{2\mu_R R^2}\right)\hat{j}^2 + \frac{1}{2\mu_R R^2}(\hat{J}^2 - 2\hat{J}_z^2 - \hat{J}_+\hat{j}_- - \hat{J}_-\hat{j}_+) + V(r, R, \chi) \quad (1)$$

where $\hat{J}$ and $\hat{J}_z$ are, respectively, the total angular momentum and its projection on to the BF z axis, $\hat{j}$ is the rotational angular momentum of the diatom, and μ_R and μ_r are the appropriate reduced masses. The spin–orbit and electronic–rotational angular momentum couplings are ignored in this work.

The BF wavefunction is expanded as

$$\Psi^{JM}(\alpha, \beta, \gamma, r, R, \chi) = \sqrt{\frac{2J+1}{8\pi^2}}\frac{1}{rR} \times \sum_{K=-J}^{J} D^J_{KM}(\alpha, \beta, \gamma)\psi^J_K(r, R, \chi) \quad (2)$$

where (α, β, γ) are the Euler angles of rotation of the BF with respect to the SF frame, and D^J_{KM} is the rotational matrix in the notation of Edmonds.[43] The sum over K collapses if the molecule is a symmetric top, since D^J_{KM} are the eigenfunctions of the corresponding rotational Hamiltonian. Substituting eqn. (2) back into eqn. (1) and invoking the helicity decoupling approximation which ignores the K,K' coupling,[42,44–46] the reduced Hamiltonian for $\psi^J_K(r, R, \chi)$ is obtained:

$$\hat{H}^J_K = -\frac{\hbar^2}{2\mu_R}\frac{\partial^2}{\partial R^2} - \frac{\hbar^2}{2\mu_r}\frac{\partial^2}{\partial r^2} + \frac{[J(J+1) - 2K^2]\hbar^2}{2\mu_R R^2} + V(r, R, \chi) - \frac{\hbar^2}{2}\left(\frac{1}{\mu_R R^2} + \frac{1}{\mu_r r^2}\right) \times \left[\frac{1}{\sin\chi}\frac{\partial}{\partial\chi}\left(\sin\chi\frac{\partial}{\partial\chi}\right) - \frac{K^2}{\sin^2\chi}\right] \quad (3)$$

where we have used the property that D^J_{KM} is an eigenfunction of $\hat{J}^2$ and $\hat{J}_z$. The helicity decoupling scheme is particularly appropriate for the large reduced masses and small J considered here.

B Photodissociation cross-sections

Following Balint-Kurti and Shapiro,[14,15] the differential cross-section for an optical bound-to-free transition of a triatomic molecule can be written as

$$\sigma(\hat{k}Enjm_j \,|\, E_i J_i M_i K_i) = \left(\frac{4\pi^2\omega}{c}\right)|\langle\psi^{-\hat{k}njm_j}(\boldsymbol{R}, \boldsymbol{r}, E)\,|\,\hat{\boldsymbol{\varepsilon}}'\cdot\boldsymbol{\mu}'\,|\,\Psi^{J_iM_iK_i}(\boldsymbol{R}, \boldsymbol{r}, E_i)\rangle|^2 \quad (4)$$

where $\hat{\boldsymbol{\varepsilon}}'$ is a unit vector in the polarization direction of the photon and $\boldsymbol{\mu}'$ is the transition dipole vector, both in the SF frame. The initial state, given in eqn. (2) and labelled by its vibrational energy (E_i) and angular momentum quantum numbers ($J_i M_i K_i$), is a bound eigenfunction of the ground state Hamiltonian.[47] Here, the ClNO molecule is approximated by a symmetric top, which makes K_i a good quantum number. The final scattering state, labelled by the scattering angles $\hat{k} = (\theta'_k, \phi'_k)$ in the SF frame, energy ($E = E_i + \hbar\omega$), and the fragment internal state quantum numbers ($n_j m_j$), is normalized on the energy scale and expressed as:[19]

$$\psi^{-\hat{k}njm_j}(\boldsymbol{R}, \boldsymbol{r}, E) = (-1)^{j-m_j}\sum_{JMK}(-1)^K\frac{2J+1}{4\pi} \times D^{J*}_{KM}(\phi'_k, \theta'_k, 0) \times D^{j*}_{-K-m_j}(\phi'_k, \theta'_k, 0) \times D^J_{KM}(\alpha, \beta, \gamma)\zeta^{-J}_{njK}(r, R, \chi)/rR \quad (5)$$

The wavefunctions satisfy the following wave boundary condition:

$$\lim_{R\to\infty}\zeta^{-J}_{njK}(r, R, \chi) \sim \sqrt{\frac{\mu_R}{2\pi h^2 k_{nj}}}\left[\mathrm{e}^{\mathrm{i}k_{nj}R}\eta_{njK}(r, \chi) - \sum_{n'j'}\sqrt{\frac{k_{nj}}{k_{n'j'}}}S^{J*}_{njK,\,n'j'K}\,\mathrm{e}^{-\mathrm{i}k_{n'j'}R} \times \eta_{n'j'K}(r, \chi)\right] \quad (6)$$

where $S^J_{njK,\,n'j'K}$ are the S-matrix elements. The wave vector in the dissociation coordinate is $k_{nj} = \sqrt{2\mu_R(E_i + \hbar\omega - \varepsilon_{nj})}/\hbar$. and ε_{nj} is the eigenenergy of the fragment corresponding to the eigenstate $\eta_{njK}(r, \chi)$:

$$\hat{H}_{\mathrm{BC}}\eta_{njK}(r, \chi) = \varepsilon_{nj}\eta_{njK}(r, \chi) \quad (7)$$

The component of the transition dipole vector along the polarization direction in eqn. (4) is expressed[26] in spherical tensor representation:[43]

$$\hat{\boldsymbol{\varepsilon}}\cdot\boldsymbol{\mu}' = \sum_{g=-1}^{1}(-1)^g\varepsilon'_g\mu'_{-g} = \sum_{g=-1}^{1}(-1)^g\varepsilon'_g\sum_{h=-1}^{1}\mu_h D^1_{h-g} \quad (8)$$

where the dipole components in the BF frame (μ_g) are functions of the Jacobi coordinates and D^1_{h-g} is the rotational matrix.

Substituting eqn. (2), (5), and (8) into eqn. (4), the photodissociation amplitude takes the form:[19]

$$f(\hat{k}Enjm_j \,|\, E_j J_i M_i K_i) = \langle\psi^{-\hat{k}njm_j}(\boldsymbol{R}, \boldsymbol{r}, E)\,|\,\hat{\boldsymbol{\varepsilon}}'\cdot\boldsymbol{\mu}'\,|\,\Psi^{J_iM_iK_i}(\boldsymbol{R}, \boldsymbol{r}, E_i)\rangle = (-1)^{j-m_j}\sum_{JMK}(-1)^K\sqrt{\frac{2J+1}{4\pi}}D^J_{KM}(\hat{k}) \times D^j_{-K-m_j}(\hat{k})\sum_{gh}(-1)^g\varepsilon'_g \times w(JMK\,|\,hg\,|\,J_iM_iK_i)t(EJKnj\,|\,h\,|\,E_iJ_iK_i) \quad (9)$$

in which the integral over the three Euler angles is straightforward[43]

$$\begin{aligned} w(JMK\,|\,hg\,|\,J_i M_i K_i) &= \sqrt{\frac{2J+1}{8\pi^2}}\sqrt{\frac{2J_i+1}{8\pi^2}}\int_0^{2\pi}\mathrm{d}\alpha\int_0^{\pi}\sin\beta\,\mathrm{d}\beta\int_0^{2\pi}\mathrm{d}\gamma \\ &\quad\times D^{J*}_{KM}(\alpha\beta\gamma)D^{J_i}_{K_iM_i}(\alpha\beta\gamma)D^{1}_{h-g}(\alpha\beta\gamma) \\ &= \sqrt{(2J+1)(2J_i+1)}(-1)^{K-M} \\ &\quad\times\begin{pmatrix} J & J_i & 1 \\ -K & K_i & h\end{pmatrix}\begin{pmatrix} J & J_i & 1 \\ -M & M_i & -g\end{pmatrix} \end{aligned} \tag{10}$$

where the properties of the 3-j symbols determine the selection rules:

$$J = J_i,\ J_i \pm 1,\ K = K_i + h, \text{ and } M = M_i - g$$

To simplify the above formula, we assume that the external field is polarized along the SF z' axis, hence $g = 0$ and M is conserved.

The integral over the Jacobi coordinates

$$\begin{aligned} t(EJKnj\,|\,h\,|\,E_i J_i K_i) &= \int_0^{\infty}\mathrm{d}r\int_0^{\infty}\mathrm{d}R\int_0^{\pi}\sin\chi\,\mathrm{d}\chi\,\zeta^{-J*}_{njK}(r,R,\chi) \\ &\quad\times\mu_h(r,R,\chi)\psi^{J_i}_{K_i}(r,R,\chi) \end{aligned} \tag{11}$$

obtained by wave packet propagation represents the most computationally intensive part of the calculations.

The cross-section of main experimental interest at present is the m_J-summed one:

$$\begin{aligned} \bar{\sigma}(\hat{k}Enj\,|\,E_i J_i M_i K_i) &= \sum_{m_j}\sigma(\hat{k}Enjm_j\,|\,E_i J_i M_i K_i) \\ &= \frac{4\pi^2\omega}{c}\sum_{JJ'K}\sqrt{\frac{2J+1}{4\pi}}\sqrt{\frac{2J'+1}{4\pi}}D^{J*}_{KM_i}(\hat{k})D^{J'}_{KM_i}(\hat{k}) \\ &\quad\times\sum_{hh'}w(JK\,|\,h0\,|\,J_i M_i K_i)w(J'K\,|\,h'0\,|\,J_i M_i K_i) \\ &\quad\times t^*(EJKnj\,|\,h\,|\,E_i J_i K_i)t(EJ'Knj\,|\,h'\,|\,E_i J_i K_i) \end{aligned} \tag{12}$$

The sums over the indices (hh') are superfluous due to the selection rules in eqn. (10).

Eqn. (12) contains a large body of information. The angular distribution of the final fragments provides information on the vector properties of the photodissociation process. Integration over the scattering angles (θ'_k, ϕ'_k) yields cross-sections that determine the scalar properties of the process.

C Chebyshev propagation

The key to the calculation of the photodissociation cross-sections discussed in the above section is the computation of the t matrix. In this work, we use a new and efficient scheme based on the Chebyshev propagator,[27] $T_k(\hat{H}) \equiv \cos(k\hat{\Theta})$ with $\hat{\Theta} \equiv \arccos\hat{H}$ and $\hat{H} \in [-1, 1]$. The wave packet is propagated in the Chebyshev order (k) domain, and subsequently transformed to the Chebyshev angle (θ) domain *via* a cosine Fourier transform.[48,49] Attributes in the energy domain can thus be obtained *via* a simple change of variables: $E = \cos\theta$.

The order–angle ($k-\theta$) formulation is equivalent to the well known time–energy (t–E) formulation. In fact, the order and angle can be considered as effective time and effective energy, respectively.[48] The order–angle ($k-\theta$) formulation has certain numerical advantages over the traditional time-dependent approach.[50–52] For instance, because of its polynomial form, the Chebyshev propagator can be calculated exactly using a three-term recurrence relationship, in contrast to the time propagator which can only be calculated approximately using, *e.g.* polynomial interpolations.[53] The Chebyshev propagation is extremely stable and requires minimal storage. For a Hermitian Hamiltonian and a real initial wave packet, the entire propagation can be cast in real space. Furthermore, the Chebyshev approach eliminates discretization errors present in conventional time-dependent approaches. This method has recently been applied successfully to study the photodissociation dynamics[27] and the resonant Raman spectrum[54] of a two-dimensional system, and was found to be highly efficient.

In the Chebyshev formulation, the initial rotational-state-resolved total cross-section can be rewritten as a cosine Fourier transform of the corresponding autocorrelation function in the Chebyshev angle domain:[27]

$$\sigma(\theta JK\,|\,\theta_i J_i M_i K_i) = \frac{4\pi^2\omega}{c}\frac{2}{\pi}\sum_{k=0}^{\infty}\left(1-\frac{\delta_{k0}}{2}\right)\cos(k\theta)C^{JK}_k \tag{13}$$

where

$$C^{JK}_k = \langle\Phi^{JK}_0\,|\,\Phi^{JK}_k\rangle \tag{14}$$

The initial wave packet in the propagation is the ground-state vibrational eigenstate multiplied by the transition dipole components $|\,\Phi^{JK}_0\rangle = \mu_h\,|\,\psi^{J_i}_{K_i}\rangle$, where the total angular momentum and its projection to the BF z axis are determined by eqn. (10). The wave packet is propagated by recursive application of the Hamiltonian operator:

$$|\,\Phi^{JK}_k\rangle \equiv \hat{T}_k(\hat{H})\,|\,\Phi^{JK}_0\rangle = 2\hat{H}\,|\,\Phi^{JK}_{k-1}\rangle - |\,\Phi^{JK}_{k-2}\rangle \tag{15a}$$

with

$$|\,\Phi^{JK}_1\rangle = \hat{H}\,|\,\Phi^{JK}_0\rangle,\ |\,\Phi^{JK}_0\rangle = \hat{I}\,|\,\Phi^{JK}_0\rangle \tag{15b}$$

To calculate the partial cross-sections, we note that the scattering states form a complete set

$$\sum_{n''j''}\int_{-1}^{1}\mathrm{d}\cos\theta'\,|\,\zeta^{-J}_{n''j''K}(\theta')\rangle\langle\zeta^{-J}_{n''j''K}(\theta')\,| = I \tag{16}$$

in addition to their orthogonality:

$$\langle\zeta^{-J}_{njK}(\theta)\,|\,\zeta^{-J}_{n''j''K}(\theta')\rangle = \delta_{nn''}\,\delta_{jj''}\,\delta(\cos\theta - \cos\theta') \tag{17}$$

Thus, the final wave packet can be written as a superposition of the scattering states:

$$\begin{aligned} |\,\Phi^{JK}_k\rangle &= \sum_{n''j''}\int_{-1}^{1}\mathrm{d}\cos\theta'\langle\zeta^{-J}_{n''j''K}(\theta')\,|\,\mu_h\,|\,\psi^{J_i}_{K_i}\rangle \\ &\quad\times\left(\frac{\mathrm{e}^{\mathrm{i}k\hat{\Theta}}+\mathrm{e}^{-\mathrm{i}k\hat{\Theta}}}{2}\right)|\,\zeta^{-J}_{n''j''K}(\theta')\rangle \end{aligned} \tag{18}$$

where $t(\theta' JKn''j''\,|\,h\,|\,\theta_i J_i K_i) = \langle\zeta^{-J}_{n''j''K}(\theta')\,|\,\mu_h\,|\,\psi^{J_i}_{K_i}\rangle$. As discussed above, the order and angle can be considered as effective time and effective energy, respectively. Thus, the propagation of the scattering wavefunction with the propagator ($e^{-\mathrm{i}k\hat{\Theta}}$) results in purely outgoing waves in the dissociation asymptote, while the propagator ($\mathrm{e}^{\mathrm{i}k\hat{\Theta}}$) leads to incoming waves.

For large enough k, the wave packet is completely out of the interaction region. The asymptotic wave packet consists of two parts due to the cosine propagator used here. As shown in the earlier work[27] the two parts are identical in coordinate space, but have opposite momenta. The physically relevant part in our problem is apparently the one corresponding to positive momenta in R, which is consistent with the conventional use of incoming wave boundary conditions in photodissociation problems [eqn. (6)].[14] To extract the t matrix elements, we multiply eqn. (18) on the left-hand side by the outgoing wavefunction

$$\lim_{R\to\infty}|\,\Xi^{+}_{njK}(\theta)\rangle \sim \sqrt{\frac{\mu_R}{2\pi\hbar^2 k_{nj}}}\,\mathrm{e}^{\mathrm{i}k_{nj}R}\eta_{njK}(r,\chi) \tag{19}$$

and integrate over the three Jacobi coordinates. The final result reads:

$$\lim_{k\to\infty}\langle \Xi^{+}_{njK}(\theta)\,|\,\cos(k\hat{\Theta})\,|\,\Phi_0^{JK}\rangle \propto t(\theta JKnj\,|\,h\,|\,\theta_i J_i K_i)\,\mathrm{e}^{-\mathrm{i}k\theta} \quad (20)$$

Note that the outgoing wavefunctions in eqn. (19) are orthogonal to plane waves with negative momenta (incoming waves) which appear in the second term in eqn. (6). Finally, the energy normalized cross-section is related to the angle normalized cross-section by the following relationship:

$$\sigma(E=\cos\,\theta)=\frac{1}{\sin\,\theta}\,\sigma(\theta) \quad (21)$$

D Discretization

The propagation in the Chebyshev order domain calls for repeated evaluation of the action of the Hamiltonian. The reduced Hamiltonian [eqn. (3)] is represented in a direct product discrete variable representation (DVR)[55] grid. Both the vibrational and translational degrees of freedom are discretized using the DVR of Colbert and Miller,[56] which uses sine functions as the finite basis representation (FBR). The DVR grids are defined as follows:

$$r_v = r_{\min} + (r_{\max} - r_{\min})v/N_r; \quad v = 1, \ldots, N_r - 1$$

$$R_\mu = R_{\min} + (R_{\max} - R_{\min})\mu/N_R; \quad \mu = 1, \ldots, N_R - 1$$

with which the action of the kinetic energy operator on the DVR wavefunction is proportional to the following matrix:

$$-\left\langle v\left|\frac{\mathrm{d}^2}{\mathrm{d}r^2}\,|\,v'\right\rangle = \frac{\pi^2(-1)^{v-v'}}{2(r_{\max}-r_{\min})^2}\right.$$
$$\left\{\begin{array}{ll}\dfrac{(2N_r^2+1)}{3}-\dfrac{1}{\sin^2\left[\dfrac{v\pi}{N_r}\right]}; & v=v'\\[2ex] \dfrac{1}{\sin^2\left[\dfrac{(v-v')\pi}{2N_r}\right]}-\dfrac{1}{\sin^2\left[\dfrac{(v+v')\pi}{2N_r}\right]}; & v\neq v'\end{array}\right\}. \quad (22)$$

A similar matrix applies to the R coordinate.

The angular DVR, due to Corey and Lemoine,[57] is defined on the Gauss–Legendre quadrature points $\{\chi_\kappa\}$, which are the zeros of the $(j_{\max}+1)$th $(j_{\max}=N_\chi-1)$ order Legendre polynomial $P_{j_{\max}}(\cos\,\chi)$. The corresponding FBR consists of the normalized associated Legendre functions and the transformation between DVR and FBR is given by:

$$\begin{aligned} U^K_{j\kappa} &= \sqrt{w_\kappa}\,P^K_j(\cos\,\chi_\kappa); && K\geqslant 0\\ &= \sqrt{w_\kappa}\,(-1)^{|K|}P^{|K|}_j(\cos\,\chi_\kappa); && K<0\end{aligned} \quad (23)$$

with $j=|K|, \ldots, j_{\max}$ and $\kappa=1, \ldots, j_{\max}+1$. Note that the above matrix is dependent on K and not necessarily square. The action of the rotational angular momentum operator on the DVR wave packet is replaced by multiplication by the matrix

$$\left\langle\kappa\left|\frac{-1}{\sin\,\chi}\frac{\partial}{\partial\chi}\left(\sin\,\chi\,\frac{\partial}{\partial\chi}\right)+\frac{K^2}{\sin^2\,\chi}\right|\kappa'\right\rangle = \sum_{\kappa'}\sum_{j=|K|}^{j_{\max}} U^K_{j\kappa}\,j(j+1)\,U^K_{j\kappa'} \quad (24)$$

The action of the potential-energy operator is calculated by multiplication in the coordinate domain where V is local.

III Results

In this section, we apply the method outlined in the previous section to the ClNO(S_1) photodissociation. The ground electronic state potential, taken from ref. 37, consists of three coupled quadratic potentials with the force constants fitted to spectroscopic data.[58] The excited-state potential-energy surface is adoped from the work of Manthe *et al.*[38] who fitted the *ab initio* data of Schinke *et al.*[36] The transition dipole functions are expanded in terms of spherical harmonics as

$$\mu_h(r,\,R,\,\chi)=\sum_f C_f(r,\,R)\,Y_{f-h}(\chi,\,0) \quad (25)$$

where, since the $S_0\rightarrow S_1$ transition is perpendicular, only the $h=\pm 1$ components are included. Due to the lack of information on the dependence of the dipole vector on the internal coordinates, the functions are assumed to be independent of the radial coordinates and only the first term in the angular expansion is retained. To ensure odd parity of $\hat{\boldsymbol{\varepsilon}}'\cdot\boldsymbol{\mu}'$, we choose $C_{fh}=C^*_{f-h}$.

We use an $N_r\times N_R\times N_\chi = 30\times 300\times 80$ grid for $[R_{\min}, \Delta R]=[3.9, 0.04]\,a_0$ and $[r_{\min}, \Delta r]=[1.8, 0.03]\,a_0$. In order to apply the Chebyshev propagator, the Hamiltonian $\hat{H}_0$ is scaled to $[-1, 1]$:

$$\hat{H}=\frac{\hat{H}_0-\bar{H}}{\Delta H} \quad (26a)$$

where the midpoint and halfwidth

$$\bar{H}=(H_{\max}+H_{\min})/2, \quad \Delta H=(H_{\max}-H_{\min})/2 \quad (26b)$$

are estimated from the grid. The propagation typically requires about 1100 Chebyshev steps, although the calculation of the total cross-section needs many less steps. The ground ro-vibrational state of the ClNO molecule in the ground electronic state is obtained using the relaxation method of Kosloff and Tal-Ezer,[59] which forces the system to converge to the lowest energy state by using an exponential filter. The energy of the ground ro-vibrational state is 1361 cm^{-1}, in good agreement with the experimental value.[58]

As discussed above, the wave packet in the Chebyshev order domain is real, since both the ground vibrational state and the dipole functions are real. Fig. 1 shows the motion of the wave packet in the r, R grid, which is obtained by averaging over the angular coordinate. The initial wave packet at $k=0$ is the ground-state wavefunction multiplied by the transition dipole function. It can be readily seen that the wave packet is relatively compact throughout the dissociation and moves down hill, much like the time-dependent wave packet.[37] Motion of the wave packet in the vibrational coordinate during the dissociation can be attributed to the vibrational excitation in the N—O mode. The oscillatory structure of the asymptotic wave packet in the R coordinate is due to the interference among the plane waves.

A Total cross-section

Fig. 2 displays the autocorrelation function in the Chebyshev order domain for the dissociation of ClNO(S_1) with J, $K=1$,

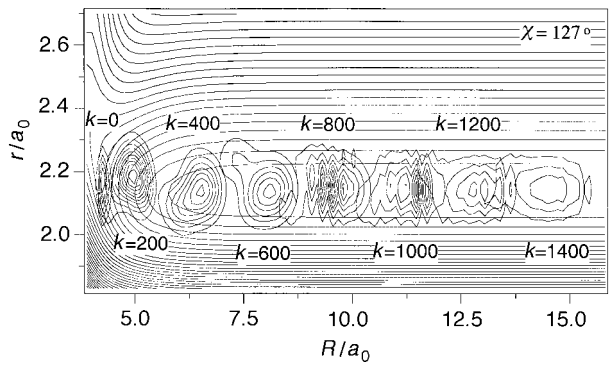

Fig. 1 Wave packet motion on the two-dimensional r, R grid. The wave packet is superimposed on the excited state potential-energy surface at $\chi=127°$.

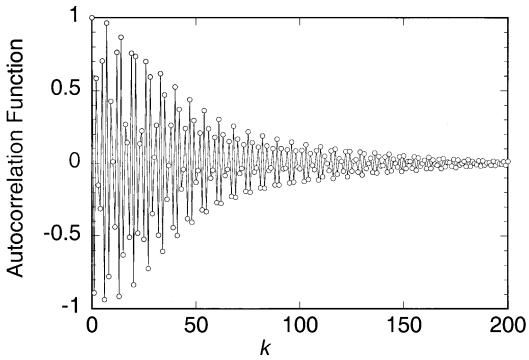

Fig. 2 Autocorrelation function in the Chebyshev order domain. The line connecting the points is included to guide the eyes.

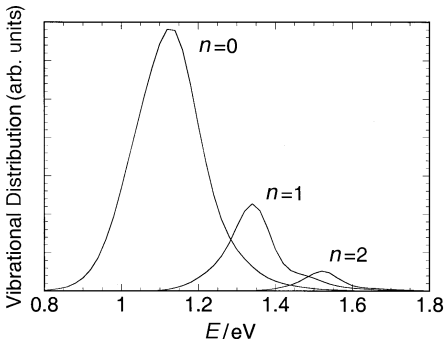

Fig. 4 Energy dependence of the NO vibrationally resolved partial cross-sections for the lowest three vibrational states.

0. The correlation function, which contains the frequency information, oscillates between 1 and −1. Since the system is near the bottom of the normalized energy span (*ca.* −1), which corresponds to a Chebyshev angle (θ) near π, increasing k by one unit leads, roughly speaking, to a sign change in the correlation function. The envelope of the oscillations decreases with k monotonically, indicating that the wave packet moves out of the Franck–Condon region. By $k = 200$, the wave packet already has a very small overlap with the initial wave packet, which can also be seen in Fig. 1. A cosine Fourier transform of the correlation function [eqn. (13)] recovers the total cross-section, which is displayed in Fig. 3. It is very similar to those reported by Untch *et al.*[37] and by Manthe *et al.*,[38] who considered the dissociation with zero total angular momentum. The rather weak dependence of the absorption spectrum on the rotational quantum numbers of the parent molecule is due to the rapid nature of the process and the small initial angular momentum considered. The shape of the cross-section reflects the dynamics in the Franck–Condon region. As pointed out before,[37] the smeared peaks at the high-energy side can be identified with the excitation to the overtones of the N—O stretch mode in the parent molecule in the initial excitation.

B Vibrationally and rotationally resolved partial cross-sections

The partial cross-sections are much more sensitive to the details of the potential-energy surface, thus yielding more information on the dynamics. In this work, we calculate the partial cross-sections using approximate internal state wavefunctions for the NO fragment: $\eta_{njK}(r, \chi) \approx \phi_n(r)P_j^K(\chi)$. The projection was done at $k = 1150$, where the wave packet is completely out of the interaction region (see Fig. 1). The energy dependence of the vibrationally resolved partial cross-sections is displayed in Fig. 4 for the first three vibrational states of NO. It can be readily seen that these partial cross-sections correspond to the first three peaks in the total cross-section shown in Fig. 3. Indeed, the vibrational excitation of the NO fragment originates from the initial excitation of the parent molecule and the dissociation is nearly vibrationally adiabatic.[37] In Fig. 5, the energy dependence of rotationally resolved partial cross-sections is presented for some NO rotational states. These cross-sections are all dominated by a main peak near the centre of the absorption spectrum. As energy increases, higher rotational states become more dominant. Direct comparison can be made with experimental measurements by Reisler and co-workers,[34] who obtained several partial cross-sections as functions of the excitation wavelength. As discussed in previous calculations,[37] the agreement is good. The sum of the partial cross-sections gives a very good agreement with the total cross-section obtained directly from the autocorrelation function, which reinforces the self-consistency of the calculation.

The normalized rotational distributions for the first three NO vibrational states are given in Fig. 6 for three different energies corresponding roughly to the peak positions of the vibrational structure in the absorption spectrum (Fig. 4). It can be seen that these distributions are highly inverted. As extensively discussed earlier,[36,37] the excitation of the fragment rotational degree of freedom can be attributed to the strong anisotropy of the potential energy surface in the exit channel, which exerts a large torque on the departing NO. The distributions are typically Gaussian-shaped inside the energy ranges defined by their own vibrational excitation profiles (Fig. 4), but show oscillatory structures outside these ranges. In fact, the rotational distributions for $n = 0$, 1 at $E = 1.15$ eV are very similar to those for $n = 1$, 2 at $E = 1.35$ eV. The Gaussian shape of the distribution can be readily interpreted by the rotational reflection principle,[60] while the oscillatory structure is probably due to interferences.[37] The peak position moves to higher j with increasing photon energy, in contrast to the experimental observation of weak wavelength dependence.[33] The disagreement is likely to be the result of an imperfect potential-energy surface. The calculated

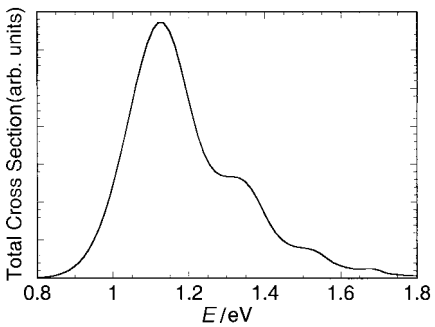

Fig. 3 Total cross-section of the ClNO dissociation in the first singlet-excited state.

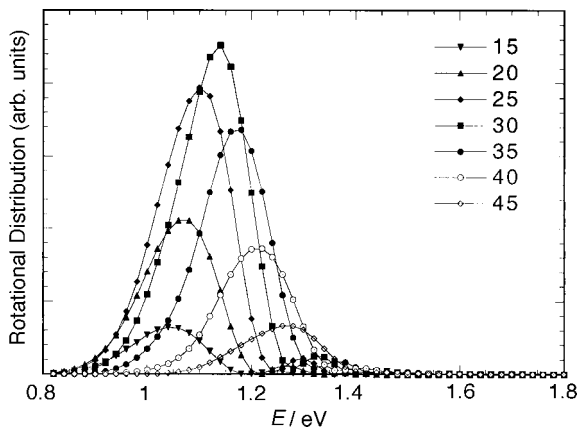

Fig. 5 Energy dependence of partial cross-sections for some NO rotational states of the ground vibrational level ($n = 0$).

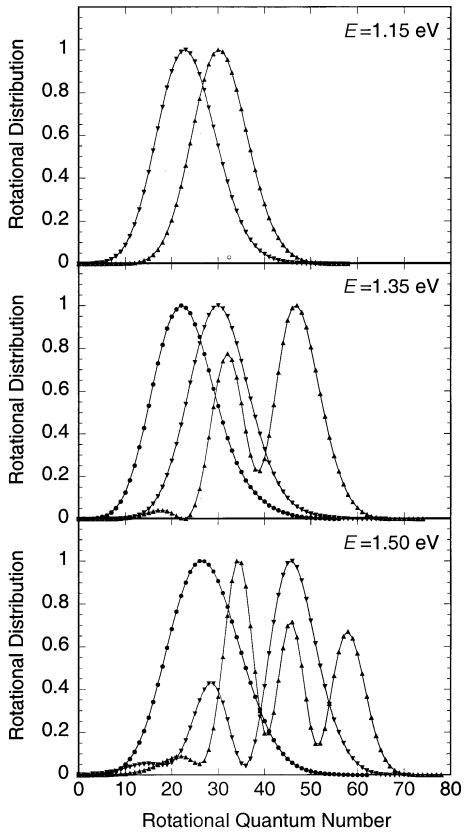

Fig. 6 Normalized rotational state distributions of NO for $J, K = 1$, 0 at three different energies. The ground, first and second excited vibrational states of NO are denoted by (▲), (▼) and (●), respectively.

distributions are otherwise in good agreement with experimental measurements. Near the peak of the absorption spectrum, for example, the calculated peak position and FWHM width for the rotational distribution for the vibrational ground state of the NO fragment is $j = 30$ and 13, compared with the experimental values of 30.5 and 10 ± 1.[34] The rotational distributions obtained in this work are similar to those reported by Untch *et al.*,[37] but there are some quantitative differences because the potential-energy surface used in this work is a different fit[38] to the *ab initio* data.[36] Our rotational distributions are, for example, typically more excited than those obtained by Untch *et al.*,[37] improving the agreement with experimental data. However, it should be stressed that this improvement is not due to the inclusion of the overall rotation of the parent molecule (see below).

Interestingly, the NO rotational distributions are insensitive to the overall rotation of the parent molecule. In fact, the partial cross-sections are practically the same for the different J and K used in the calculation. This result can be expected since the torque experienced by the departing NO fragment is sufficiently strong to overwrite the differences in parent rotation. To put in perspective, the average rotational energy of the NO fragment is *ca.* 1500 cm^{-1} while the parent rotational energy is of the order of 1 cm^{-1}. If the dissociation process is considered as a half-collision with the Franck–Condon region as the transition state, the energy disparity translates to a negligible energy shift in reaction probability according to the J-shifting approximation.[61] The insensitivity to overall rotation further justifies the helicity decoupling approximation used in our dynamical model. It should be pointed out, however, that rather different results are expected for systems with small to moderate product rotational excitation, where the overall rotation may make a significant difference.[62] Of course, parent rotation plays a much more important role for higher rotational states of the molecule.

C Angle-resolved partial cross-sections

In this section, we concentrate on the angle-resolved partial cross-sections for dissociation out of $J_i M_i K_i$ selected parent molecules. First, we consider the trivial case, where the initial rotational quantum numbers are J_i, M_i, $K_i = 0, 0, 0$. This state cannot be selected using an electric hexapole and is included here mainly for pedagogical purposes. The selection rules for a perpendicular transition would allow the following final angular momenta: $J = 1$, $K = \pm 1$. The m_J-summed cross-section can thus be expressed as

$$\bar{\sigma}(\hat{k}\,|\,000) = \frac{3\pi\omega}{2c} \sin^2\theta'_k[w(101)^2\,|\,t(11)\,|^2 + w(10-1)^2\,|\,t(1-1)\,|^2] \quad (27)$$

where we have used reduced notations for $t(JK)$ and $w(JKM)$. As discussed before,[19] the trivial case is equivalent to the well known[63] M_i-averaged cross-section $\bar{\bar{\sigma}} \propto 1 + \beta P_2(\cos\theta'_k)$, where P_2 is the second-order Legendre polynomial. For a perpendicular transition ($\beta = -1$), it exhibits the familiar $\sin^2\theta'_k$ structure. Fig. 7 displays the angle-resolved partial cross-sections for a number of product states. They all have the same shape that maximizes in the direction perpendicular to the polarization vector of the photon. The relative intensities are modulated entirely by the final product distributions and the t matrix is nearly independent of the initial angular momentum quantum numbers.

Next, we consider a scenario more relevant to the situation under experimental consideration,[41] *i.e.* J_i, M_i, $K_i = 1, 1, -1$. Angular momentum selection rules allow $J = 1$, $K = 0$ and $J = 2$, $K = 0, -2$ for the excited state. The cross-section has the following form:

$$\begin{aligned}\bar{\sigma}(\hat{k}\,|\,11-1) = \frac{\pi\omega}{c}\{&\tfrac{3}{2}\sin^2\theta'_k\,w(110)^2\,|\,t(10)\,|^2 \\ &+ \tfrac{15}{2}\sin^2\theta'_k\,w(210)^2\,|\,t(20)\,|^2 \\ &+ \tfrac{5}{4}\sin^2\theta'_k(\cos\theta'_k - 1)^2 w(21-2)^2\,|\,t(2-2)\,|^2 \\ &+ \sqrt{45}\sin^2\theta'_k\cos\theta'_k\,w(110) \\ &\times w(210)\mathrm{Re}[t^*(10)t(20)]\}. \end{aligned} \quad (28)$$

The common $\sin^2\theta'_k$ term in the above expression ensures that the angular distributions decay to zero at 0° and 180°, consistent with a perpendicular transition. Again, the shape of the angular distribution is independent of the final product state and we only display the distribution for a single product state in Fig. 8. As shown in the figure, the distribution peaks near 130° from the initial photon polarization.

Clearly, these asymmetric angular distributions cannot be described by the $1 + \beta P_2(\cos\theta'_k)$ form since the initial state is not isotropically oriented. In fact, it is the orientation of the parent molecule in the SF frame, *i.e.* $M_i = 1$, that is

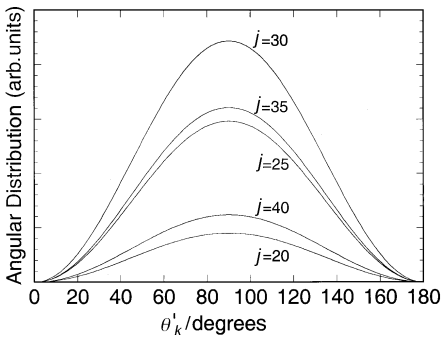

Fig. 7 Angle-resolved partial cross-sections for five NO rotational states of the ground vibrational level at $E = 1.15$ eV. The initial state is the ground vibrational J_i, M_i, $K_i = 0, 0, 0$ level of ClNO.

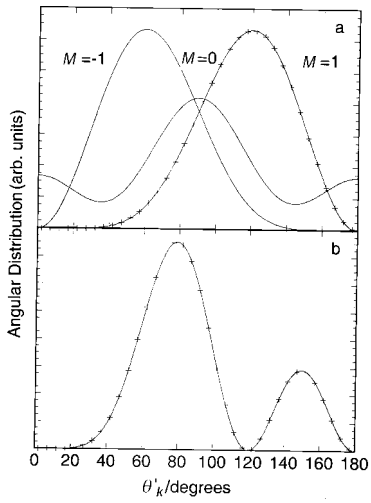

Fig. 8 Angle-resolved partial cross-sections for the J_i, M_i, $K_i = 1$, M, 1 (a) and 2, -1, 1 (b) levels of ClNO. The angular distributions given by eqn. (29), denoted by (+), agree very well with the results obtained from the full dynamical calculation.

responsible for the asymmetry. To illustrate this point, we plot, in Fig. 8, the angular distributions for two other initial magnetic quantum numbers for $J_i = 1$. It can be seen that the angular distribution for $M_i = -1$ is just the mirror image of that for $M_i = 1$, and peaks near 50°. The distribution for $M_i = 0$ is symmetric with respect to $\theta'_k = 90°$, and has a much smaller amplitude due to the unfavourable position of the parent molecule relative to the SF z' axis. The angular distribution summed over all the M_i states takes, of course, the $1 + \beta P_2(\cos\theta'_k)$ form.[14]

As analytically shown in ref. 26, when the t matrix elements are independent of J and K [within the (J, K) range allowed for a given initial state] the angular distribution takes the form

$$\bar{\sigma}(\hat{k}\,|\,J_i M_i K_i) \propto (2J_i + 1)[d^{J_i}_{K_i M_i}(\theta'_k)]^2[1 + \beta P_2(\cos\theta'_k)] \quad (29)$$

showing explicitly that the cross-section contains, in addition to the information contained in M_i-averaged angular distributions, only information about the initially selected state. The approximation invoked in deriving eqn. (29) is equivalent to assuming the dynamics is direct and extremely fast,[26] which is the case for the system discussed here. The product angular distributions are thus completely determined by the initial orientation of the parent molecule and the electric dipole selection rules. In other words, the dissociation is so prompt relative to the rotation of the system that it can be treated as a sudden event. The angular distribution given by eqn. (29) for the J_i, M_i, $K_i = 1$, 1, -1 state is plotted as '+' in Fig. 8 and shown to reproduce faithfully the cross-section of eqn. (28) which contains the full dynamics.

Finally, we consider the angular distribution following excitation of the J_i, M_i, $K_i = 2$, 1, -1 state. The analytical expression for the angular distribution is somewhat cumbersome and not given here. The angle-resolved partial cross-section is also displayed in Fig. 8. The distributions have two peaks at *ca.* 90° and *ca.* 150°, but decay to zero near 0° and 180°. Again, the angular distributions can be accurately described by eqn. (29), corresponding to the limit in which the dissociation is direct and fast.

The above results may be compared with those for the photodissociation of ammonia near the onset of predissociation, which is a slow process, evolving on two non-adiabatically coupled electronic states and with an excited-state barrier. In the latter case, the magnetic-state-selected angular distributions are expected and were in fact found[25] to differ markedly from the limit of eqn. (29), providing a sensitive probe of the dissociation dynamics, the potential-energy surfaces and the transition dipole vector.

IV Conclusion

The maximum information about photodissociation dynamics that can be derived from energy domain measurements is contained in differential cross-sections with parent energy-level- and magnetic-state-resolution and with product energy-level- and possibly magnetic-state-resolution. These cross-sections reveal both the scalar properties that are determined by the dissociation dynamics in the BF frame, and the vector properties that correlate the initial orientation of the parent molecule with final recoil direction of the fragments. Although both types of information are important for achieving a complete understanding of the dynamics, the former has traditionally been the focus of theoretical scrutiny. Recent experimental achievements in selecting parent molecule quantum states challenge theoreticians to develop and apply theoretical methods capable of extracting the information from better selected and resolved observables.

In this work, we study the full-dimensional photodissociation dynamics of ClNO(S_1) using an efficient quantum mechanical method. To that end, we introduce a new propagation scheme, which combines the required efficiency and accuracy and is expected to be useful also for higher-dimensional problems. Our choice of system has been motivated by ongoing experiments in Baugh's laboratory,[41] which illustrated the possibility of selecting single (JMK) quantum states of ClNO using an electric hexapole and measuring the angle-resolved product states distributions.

The treatment of the dynamics is approximated by the decoupling of the helicity wave packets, a scheme expected to be quite accurate for the system under investigation. Calculations are carried out for excitations from the ground vibrational state on the ground electronic state and with different initial rotational quantum numbers J_i, M_i, K_i. We discuss observables of increasing levels of detail, starting with the total cross-section, which probes essentially only the Franck–Condon region and concluding with magnetic-state-selected angular distributions which probe sensitively the electronic structure and fragmentation dynamics as well as the orientation of the initial state. Our results indicate that the overall rotation of the parent molecule has, for the low initial J considered, a very limited impact on the scalar properties such as the total and partial cross-sections, due largely to the strong fragment rotational excitation and vibrational adiabaticity. However, the fragment angular distributions are found to depend sensitively on the initial rotational quantum numbers. While the fragments exit perpendicularly to the excitation photon polarization for the J_i, M_i, $K_i = 0$, 0, 0 initial state, the angular distributions for the dissociation from the J_i, M_i, $K_i = 1$, 1, -1; 1, 1, 1; and 2, 1, -1 states are asymmetric with respect to $\theta'_k = 90°$, reflecting the orientation of the parent state.

The photodissociation of ClNO is a rapid process evolving on a single excited surface. Such processes can be readily distinguished experimentally by comparing the observed distributions with those predicted by eqn. (29), which requires no dynamical information.[26] The cross-section in that limit contains little information about the fragmentation process beyond that contained in magnetic-state-averaged cross-sections.[26] It does, however, probe the orientation of the initial state, of interest, *e.g.* for stereodynamical studies or characterization of the molecular beam. In the more general case of slower and more complex fragmentation dynamics,[25] and in problems where the transition dipole varies significantly with coordinates (as is typical, for instance, in the presence of non-adiabatic interactions) the M_i-selected angular

distribution probes sensitively the dissociation dynamics and maps the transition dipole function.[19] In such scenarios, information about the parent-state orientation is entangled with information about the excited state dynamics and its analysis requires the complete, dynamical calculation. In future studies we hope to combine the numerical scheme presented here with measurements to both types of fragmentation processes in large polyatomic systems.

Acknowledgements

We thank Delroy Baugh for providing us with results of ongoing experiments and for many interesting conversations, and Uwe Manthe for sending us the potential-energy function. HG acknowledges financial support from the National Science Foundation and the Petroleum Research Fund, and some interesting discussions with Rongqing Chen.

References

1 P. R. Brooks, *Science*, 1976, **193**, 11.
2 D. H. Parker and R. B. Bernstein, *Annu. Rev. Phys. Chem.*, 1989, **40**, 561.
3 F. Harren, D. H. Parker and S. Stolte, *Comm. At. Mol. Phys.*, 1991, **26**, 109.
4 C. T. Rettner and R. N. Zare, *J. Chem. Phys.*, 1982, **77**, 2416.
5 H. J. Loesch and A. Remscheid, *J. Chem. Phys.*, 1990, **93**, 4779.
6 B. Friedrich and D. R. Herschbach, *Nature* (*London*), 1991, **353**, 412.
7 M. P. Sinha, C. D. Caldwell and R. N. Zare, *J. Chem. Phys.*, 1974, **61**, 491.
8 D. R. Pullman, B. Friedrich and D. R. Herschbach, *J. Chem. Phys.*, 1990, **93**, 3224.
9 C. Wittig, S. Sharpe and R. A. Beaudet, *Acc. Chem. Res.*, 1988, **21**, 341.
10 J. C. Polanyi and R. J. Williams, *J. Chem. Phys.*, 1988, **88**, 3363.
11 J. V. Setzler, H. Guo and G. C. Schatz, *J. Phys. Chem. B*, 1997, **101**, 5352.
12 T. Seideman, *J. Chem. Phys.*, 1995, **103**, 7887.
13 B. Friedrich and D. Herschbach, *Chem. Phys. Lett.*, 1996, **262**, 41.
14 G. G. Balint-Kurti and M. Shapiro, *Chem. Phys.*, 1981, **61**, 137.
15 G. G. Balint-Kurti and M. Shapiro, in *Photodissociation and Photoionization*, ed. K. P. Lawley, Wiley, 1985, p. 403.
16 S. R. Gandhi, T. J. Curtiss and R. B. Bernstein, *Phys. Rev. Lett.*, 1987, **59**, 2951.
17 D. Y. Kim, N. Brandstater, L. Pipes, T. Garner and D. Baugh, *J. Phys. Chem.*, 1995, **99**, 4364.
18 J. W. G. Mastenbroek, C. A. Taatjes, K. Nauta, M. H. M. Janssen and S. Stolte, *J. Phys. Chem.*, 1995, **99**, 4360.
19 T. Seideman, *J. Chem. Phys.*, 1995, **102**, 6487.
20 E. A. Torres, D. Y. Kim, L. C. Pipes, D. A. Baugh and T. Seideman, *J. Chem. Soc., Faraday Trans.*, 1997, **93**, 931.
21 C. H. Greene and R. N. Zare, *Annu. Rev. Phys. Chem.*, 1982, **33**, 119.
22 M. D. Morse, Y. B. Band and K. F. Freed, *J. Chem. Phys.*, 1983, **78**, 6066.
23 J. A. Beswick, M. Glass-Maujean and O. Roncero, *J. Chem. Phys.*, 1992, **96**, 7514.
24 H. Wei and T. Carrington, *J. Chem. Phys.*, 1996, **105**, 141.
25 T. Seideman, *J. Chem. Phys.*, 1995, **103**, 10556.
26 T. Seideman, *Chem. Phys. Lett.*, 1996, **253**, 279.
27 H. Guo, *J. Chem. Phys.*, 1998, **108**, 2466.
28 C. X. W. Qian, A. Ogai, J. Brandon, Y. Y. Bai and H. Reisler, *J. Phys. Chem.*, 1991, **95**, 6763.
29 C. X. W. Qian and H. Reisler, in *Advances in Molecular Vibrations and Collision Dynamics*, ed. J. M. Bowman, JAI, Greenwich, 1991, vol. 1.
30 Y. Y. Bai, A. Ogai, C. X. W. Qian, L. Iwata, G. A. Segal and H. Reisler, *J. Chem. Phys.*, 1989, **90**, 3909.
31 A. E. Bruno, U. Bruhlmann and J. R. Huber, *Chem. Phys.*, 1988, **120**, 155.
32 A. Ticktin, A. E. Bruno, U. Bruhlmann and J. R. Huber, *Chem. Phys.*, 1988, **125**, 403.
33 A. Ogai, C. X. W. Qian, L. Iwata and H. Reisler, *Chem. Phys. Lett.*, 1988, **146**, 367.
34 A. Ogai, C. X. W. Qian and H. Reisler, *J. Chem. Phys.*, 1990, **93**, 1107.
35 J. R. Huber and R. Schinke, *J. Phys. Chem.*, 1993, **97**, 3463.
36 R. Schinke, M. Nonella, H. U. Suter and J. R. Huber, *J. Chem. Phys.*, 1990, **93**, 1098.
37 A. Untch, K. Weide and R. Schinke, *J. Chem. Phys.*, 1991, **95**, 6496.
38 U. Manthe, H-D. Meyer and L. S. Cederbaum, *J. Chem. Phys.*, 1992, **97**, 3199.
39 A. Vegiri, A. Untch and R. Schinke, *J. Chem. Phys.*, 1992, **96**, 3688.
40 H. Grinberg, K. F. Freed and C. J. Williams, *J. Chem. Phys.*, 1997, **107**, 1849.
41 D. Baugh, personal communication.
42 R. T. Pack, *J. Chem. Phys.*, 1974, **60**, 633.
43 A. R. Edmonds, *Angular Momentum in Quantum Mechanics*, Princeton University Press, Princeton, NJ, 1960.
44 P. McGuire and D. J. Kouri, *J. Chem. Phys.*, 1974, **60**, 2488.
45 M. Tamir and M. Shapiro, *Chem. Phys. Lett.*, 1975, **31**, 166.
46 G. C. Schatz and A. Kuppermann, *J. Chem. Phys.*, 1976, **65**, 4642.
47 M. Shapiro and G. G. Balint-Kurti, *J. Chem. Phys.*, 1979, **71**, 1461.
48 R. Chen and H. Guo, *J. Chem. Phys.*, 1996, **105**, 3569.
49 R. Chen and H. Guo, *J. Chem. Phys.*, 1998, **108**, 6068.
50 Y. Huang, W. Zhu, D. Kouri and D. K. Hoffman, *Chem. Phys. Lett.*, 1993, **206**, 96.
51 V. A. Mandelshtam and H. S. Taylor, *J. Chem. Phys.*, 1995, **103**, 2903.
52 S. K. Gray and G. G. Balint-Kurti, *J. Chem. Phys.*, 1998, **108**, 950.
53 H. Tal-Ezer and R. Kosloff, *J. Chem. Phys.*, 1984, **81**, 3967.
54 H. Guo, *Chem. Phys. Lett.*, 1998, **289**, 396.
55 J. C. Light, I. P. Hamilton and J. V. Lill, *J. Chem. Phys.*, 1985, **82**, 1400.
56 D. T. Colbert and W. H. Miller, *J. Chem. Phys.*, 1992, **96**, 1982.
57 G. C. Corey and D. Lemoine, *J. Chem. Phys.*, 1992, **97**, 4115.
58 J. K. McDonald, J. A. Merritt and V. F. Kalasinsky, *J. Mol. Spectrosc.*, 1986, **117**, 69.
59 R. Kosloff and H. Tal-Ezer, *Chem. Phys. Lett.*, 1986, **127**, 223.
60 R. Schinke and V. Engel, *Faraday Discuss., Chem. Soc.*, 1986, **82**, 125.
61 J. M. Bowman, *Adv. Chem. Phys.*, 1985, **61**, 115.
62 A. R. Offer and G. G. Balint-Kurti, *J. Chem. Phys.*, 1994, **101**, 10416.
63 R. Bershon and S. H. Lin, *Adv. Chem. Phys.*, 1969, **16**, 67.

Paper 8/06792I